A Fast Approach for Preparation of Adsorbent from Reed Black Liquor and Its Performance in Equilibrium and Kinetic Gas Separation

G. Yang,[a,#] Y. Sun,[a,b,*,#] C. Wen,[c] and J. P. Zhang[a]

[a]National Engineering Laboratory of Hydrometallurgical Cleaner Production Technology, Institute of Process Engineering, Chinese Academy of Sciences, Beijing, 100190, China

[b]Edith Cowan University, School of Engineering, 270 Joondalup Drive Joondalup WA 6027 Australia

[c]School of Information Science and Technology, Northwest University, Xi'an, 710069, China

doi: 10.15255/CABEQ.2013.1856

Original scientific paper
Received: September 4, 2013
Accepted: July 27, 2015

A new approach using reed pulping black liquor by hydrothermal reaction followed by fast carbonization at 350 °C in fluidized bed reactor for 5 minutes was proposed in this paper. The BET specific surface area generated at optimum conditions reached 390 $m^2\ g^{-1}$. The CO_2 selectivity over CH_4 and N_2 comparable to commercial activated carbons was obtained. The isosteric enthalpies of adsorption for CO_2, CH_4 and N_2 on the resultant carbon sample prepared at optimum conditions show surface heterogeneity. The kinetic results indicate its potential for separation of carbon dioxide from carbon dioxide/methane mixture.

Key words:
reed, black liquor, carbon adsorbent, kinetic CO_2/CH_4 separation

Introduction

With the growing demand for paper pulp in developing countries such as China, production of paper using reed as a resource is regarded as one of the most profitable approaches for high-value conversion of biomass due to the shortage of wood-derived resources in China.[1,2] However, the major technical hurdle of non-wood pulping is the severe environmental pollution caused by the black liquid due to poor performance of alkaline recovery.[3] Exploring new approaches besides alkaline recovery for effective utilization of this hazardous material has attracted much attention. Processing routes, such as steam water gasification,[4] supercritical water gasification[5] and pyrolysis[6] have been extensively studied. Among those processes, hydrothermal carbonization of black liquor is an approach to effectively decrease COD (Chemical Oxygen Demand) and biomass content in black liquor with relatively little environmental impact.[7] The obtained carbons from hydrothermal carbonization have been reported to be utilized as solid fuels.[8] Preparation of adsorbents from hydrothermal carbonization is also a good approach for high-value conversion of biomass in aqueous solution.[7] However, the specific surface area of the carbon from hydrothermal reaction is generally low, which significantly limits its application.[7] In order to further increase the specific surface area of adsorbent, the thermal carbonization treatment will be generally applied. The most common reactor for thermal carbonization is the fixed bed reactor, which usually has rather high carbonization temperature and long reaction time. In the present work, the fluidized bed reactor was employed for thermal carbonization due to its yielding of uniform product, because of its efficient heat and mass transfer that minimize temperature variation and ensure good mixing.[9] These advantages are so compelling that the application of a fluidized bed reactor for the carbonization step can be very attractive for carbon-based adsorbent production. In addition, to the best of our knowledge, the study of a fast approach for preparation of carbon adsorbents from reed black liquor with large specific surface area and their direct application for gas separation has not been reported as yet.

Experimental section

Preparation of carbon adsorbent

The adsorbent was produced by hydrothermal reaction of 150 mL black liquor from pulping of reed in an autoclave at 200 °C for 48 hours, which

*Corresponding author: email: y.sun@ecu.edu.au, ysunipecas@gmail.com; tel: +61 (08) 6304 5931.

#The author in this paper has equal (experiment/simulation) contribution to this work.

is optimized time for relatively high yield of carbon adsorbent. The detailed pulping conditions of black liquor could be found in our previous work.[3,10] The products from the reaction were then filtered and sieved to about 0.15–0.3 mm in size after oven-drying at 110 °C for 4 hours. The solids were then carbonized at different temperatures in fluidized bed reactor. The detailed configurations, dimensions and operational parameters can be found in our previous works.[9–11] The carbon produced from hydrothermal reaction at 200 °C is denoted as Hydro-RL-200, the carbons produced from further carbonization in fluidized bed reactor at 200 °C, 250 °C and 350 °C are denoted RL-200, RL-250 and RL-350, respectively. Table 1 lists the elementary composition of black liquor before and after carbonization, and the activated carbon prepared from fluidized bed reactor. With hydrothermal treatment, the carbon composition increased from 45 to 62 %. When the precursor was carbonized in fluidized bed, carbon composition could reach 88 %. This indicates that hydrothermal treatment and carbonization facilitate removal of volatile materials from precursors. The yield of activated carbon prepared from fluidized bed was about 40 %.

Table 1 – *Comparison of elementary compositions of different precursors*

Sample	C	H	N	O (by difference)
BLB	44	6	0.5	50
BLA	62	5	0.5	32
Activated carbon	88	0.5	0.5	10

Characterization of resultant carbon adsorbents

High-pressure adsorption measurements were conducted on a standard static volumetric method apparatus. The detailed rig information and operating conditions could be found in our previous works.[12] High-purity grade methane (99.9 %), nitrogen (99.9 %), and carbon dioxide (99 %) supplied by Jingcheng Gas Co. Ltd. were used in these measurements.

The specific surface area and porosities of the carbon samples were determined by nitrogen gas adsorption at 77 K at a saturation pressure of 1 bar using a Micromeritics ASAP 2020 Automated Gas Sorption System. Carbon samples that were activated at 150 °C, were degassed at 150 °C overnight ($1.3 \cdot 10^{-4}$ Pa) prior to gas adsorption measurements, while samples activated at 350 °C were degassed ($1.3 \cdot 10^{-4}$ Pa) overnight at 350 °C. The BET surface area was assessed within the range of relative pressures from 0.05 to 0.3. The total pore volume was calculated by measuring the N_2 adsorbed at a relative pressure of 0.99. The average pore width was calculated based on the BJH method. Low-pressure adsorption equilibria measurements of CH_4, CO_2, and N_2 at 273, 283, and 293 K were obtained by a modified ASAP 2020 Automated Gas Sorption System.

Thermal gravimetric analysis was conducted on a Shimadzu TGA-50 instrument under a nitrogen (20 mL min^{-1}) atmosphere at a heating rate of 10 °C min^{-1}.

Surface morphology was examined using a Hitachi S-450 scanning electron microscope.

For kinetic adsorption measurements, RL-350 was processed by the commercial pellet machine to form pellets with average diameter of approximately 3.5 mm. The kinetics of gases adsorption was measured by the breakthrough curve method; pure gases were diluted by nitrogen with the gas concentration reaching 10 % v/v. A 316 stainless steel column with inner diameter of 2 cm, and 40 cm length was kept at 298 K and 2 bar during breakthrough curve experiment. The outlet concentration of the gases was measured by thermal conductivity detector.

In this paper, we used our own developed code based on open source R1 platform to solve the coupled differential equations. The numerical simulation was conducted on a PC with CPU 2.8 GHz. The CPU time of computation was found to be less than 2 minutes. The physical properties of the bed used for simulation include: adsorbent mass 40 g, bed density 0.61 kg m^{-3}, superficial velocity 1 m s^{-1}, bed voidage 0.34, adsorbent density 850 kg m^{-3}.

Results and discussion

Optimization of appropriate preparation conditions

Of the factors which affect the surface area of the carbons produced, the hydrothermal temperature and the carbonization temperature are the most important. The specific surface area of carbons produced from black liquor increases slightly with an increase in hydrothermal temperature, and a maximum BET specific surface area of approximate 100 m^2 g^{-1} was observed at 200 °C. Further increase in hydrothermal temperature does not significantly increase the carbon surface area, and thus carbons produced at 200 °C were selected for preparation of activated carbons.

Fig. 1 shows the thermogravimetric analysis curve of Hydro-BL-200 indicating that the weight loss is divided into three general stages. These stages correspond to the elimination of loosely

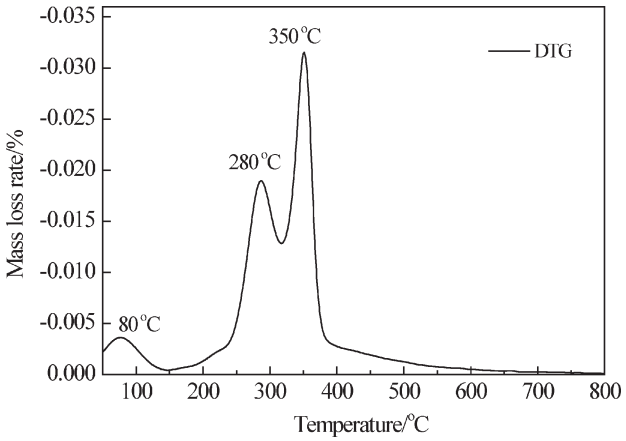

Fig. 1 – *Differential thermogravimetric analysis curve of Hydro-BL-200*

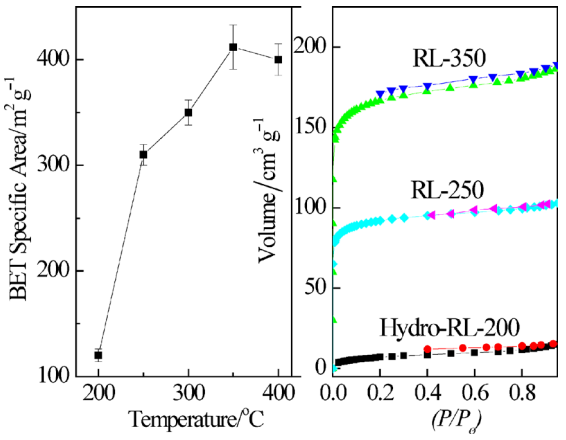

Fig. 2 – *BET specific surface area as a function of activation temperature and N_2 adsorption/desorption isotherms of different activated carbon samples*

bound moisture at around 100 °C (stage 1), the elimination of fixed water around 280 °C (stage 2), and the degradation and elimination of organic polymers around 350–450 °C (stage 3).[13] In this work, Hydro-BL-200 was carbonized at different temperatures in fluidized bed reactor. Fig. 2 indicates that the carbonization treatment significantly increases the surface area when the carbonization temperature exceeds 350 °C, at which stage the specific surface area of the carbon (RL-350) reaches around 390 m^2 g^{-1}. In terms of nitrogen adsorption isotherms, according to Brunauer-Deming-Deming-Teller (BDDT) classification,[14] the RL-350 exhibits a type I isotherm. The adsorption occurs at relatively low pressure, indicating the existence of micropores. The nitrogen adsorption/desorption isotherm of RL-350 is greater than that of Hydro-RL-200 indicating that the increased pore volume is mainly due to the removal of volatile materials during the carbonization of Hydro-RL-200 in fluidized reactor. Fig. 3 shows pressure drop and burn-off rate of Hydro-RL-200 as a function of carbonization time in the fluidized bed at 350 °C. It shows that the burn-off rate does not change appreciably after the first 5 minutes of carbonization, neither does the pressure drop. This means that, after the volatile matter had been completely removed in the first 5 minutes of carbonization, the volatilization was largely reduced. In this paper, we adopted 350 °C and 5 minutes as optimum carbonization temperature and reaction time in fluidized bed reactor.

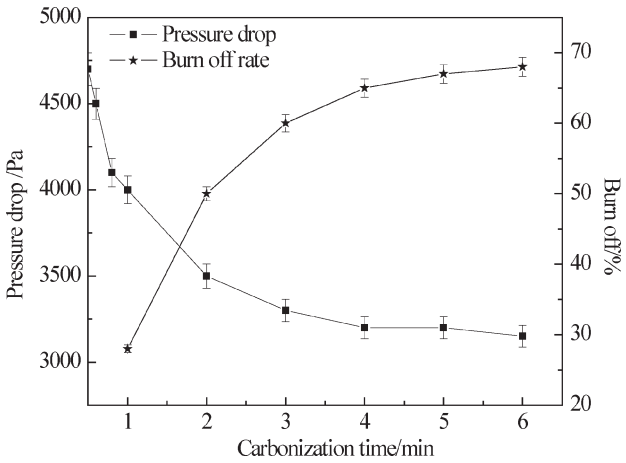

Fig. 3 – *Pressure drop and burn off as function of carbonization time*

Characterization of the resulting carbons

The pore size distribution (NLDFT, Non-Linear Density Functional Theory) assuming slit pore geometry) of RL-350 is shown in Fig. 4. The results indicate that RL-350 has a narrow pore size distribution, which mainly distributes in the microporous region in the range of 0.6~1.2 nm. In addition, it

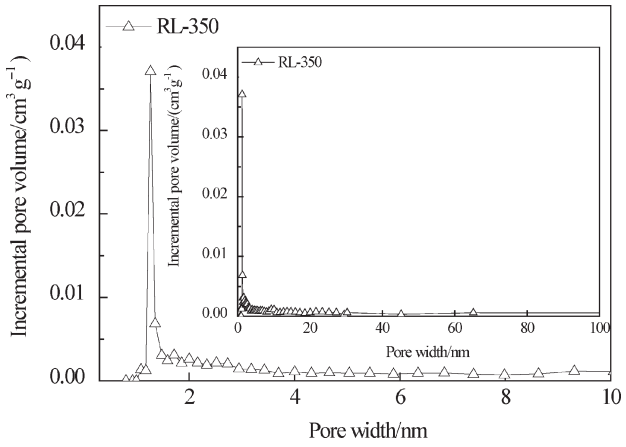

Fig. 4 – *DFT pore size distribution in microporous and mesoporous region of RL-350*

also possesses pores that belong to mesoporous region (>2 nm). The porosity parameters obtained from N_2 adsorption on RL-350 are summarized as follows: pore volume is 0.16 m^3 g^{-1}, micropore area

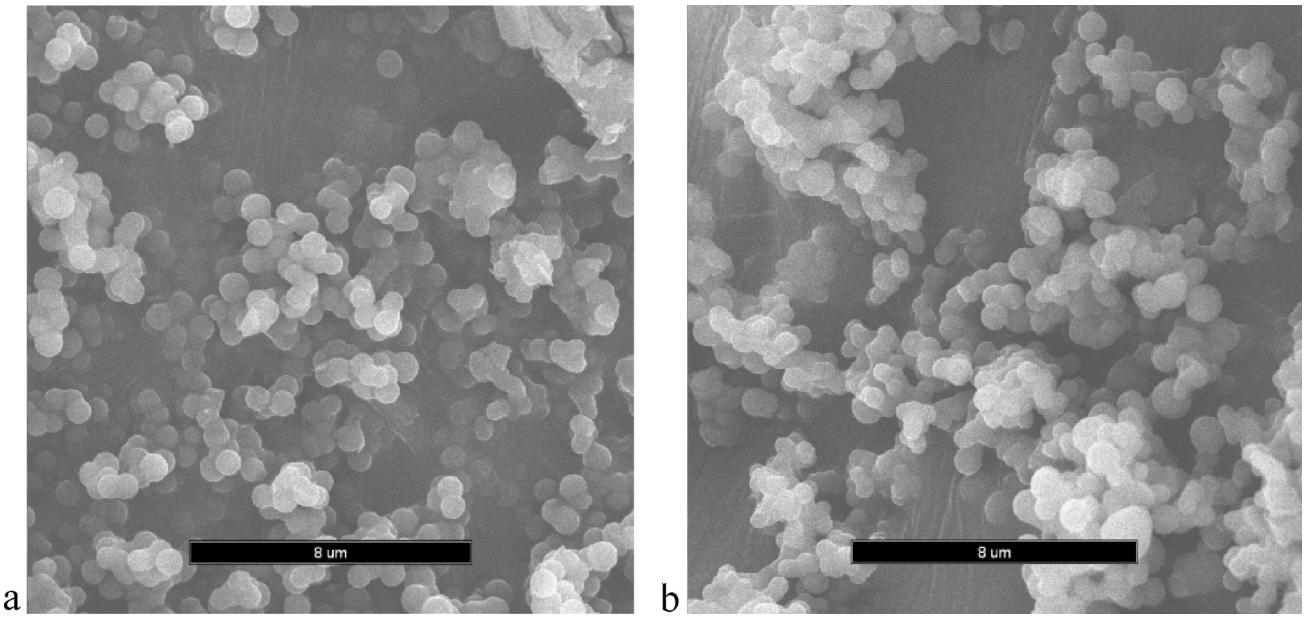

Fig. 5 – *Scanning electron microscopy images of different carbons, where a) refers to Hydro-BL-200, b) refers to RL-350*

is 270 m^2 g^{-1} and average pore width is 2.04 nm. The SEM morphology of Hydro-RL-200 and RL-350 is shown in Fig.5 a and b, respectively. Both Hydro-BL-200 and RL-350 carbons are seen to have relatively irregular carbon spheres. In addition, each carbon sphere tends to aggregate and form larger particles. After Hydro-BL-200 was carbonized in fluidized bed reactor, a further tendency of aggregation and forming of large porous particles was also observed. This suggests that the carbonization facilitates removal of volatile materials and formation of larger particles with intra-spaces, which in turn contributes to the increase in specific surface area of the resultant carbons. This result agrees with that of BET specific surface area analysis, in which the specific surface area of RL-350 significantly increased.

Low-pressure adsorption of CO_2, CH_4, and N_2

The adsorption isotherms of different gases onto RL-350 are shown in Fig. 6. The Tóth equation[15] is used to correlate our experimental low-pressure equilibrium data of different gases.

The Tóth equation is as follows:

$$q = \frac{q_m^* P}{(b + P^t)^{\frac{1}{t}}} \tag{1}$$

where q_m^* is the adsorption saturation capacity (mmol g^{-1}), b and t are the constants in Tóth equation. The constants obtained from the Tóth model are listed in Table 2.

The enthalpy of adsorption is a significant property for characterization of the type of adsorption and degree of heterogeneity of a surface. The isosteric enthalpies of adsorption were not measured experimentally in this paper, but were estimated from the low-pressure adsorption equilibrium data by using the Clausius-Clapeyron equation:

$$\Delta H = RT^2 \left(\frac{d \ln P}{dT} \right)_n \tag{2}$$

By using the low-pressure adsorption equilibrium data, we calculated the isosteric enthalpy of adsorption of RL-350 for CO_2, CH_4, and N_2, shown in Fig. 7. The isosteric enthalpy of adsorption of all the samples decreases with increase in loading be-

Table 2 – *Constants of Tóth model for adsorption of CO_2, N_2 and CH_4 onto RL-350 below 1 atm*

RL-350	Temperature	B^0	t	q_m^*
Gas	K	atm		mmol g^{-1}
CO_2	273	$4 \cdot 10^{-2}$	0.4	93
	283	$3 \cdot 10^{-2}$	0.4	80
	293	$2 \cdot 10^{-2}$	0.4	71
CH_4	273	$6 \cdot 10^{-3}$	0.7	43
	283	$5 \cdot 10^{-3}$	0.7	41
	293	$4 \cdot 10^{-3}$	0.8	33
N_2	273	$4 \cdot 10^{-3}$	1.3	19
	283	$3 \cdot 10^{-3}$	2.0	14
	293	$2 \cdot 10^{-3}$	1.1	12

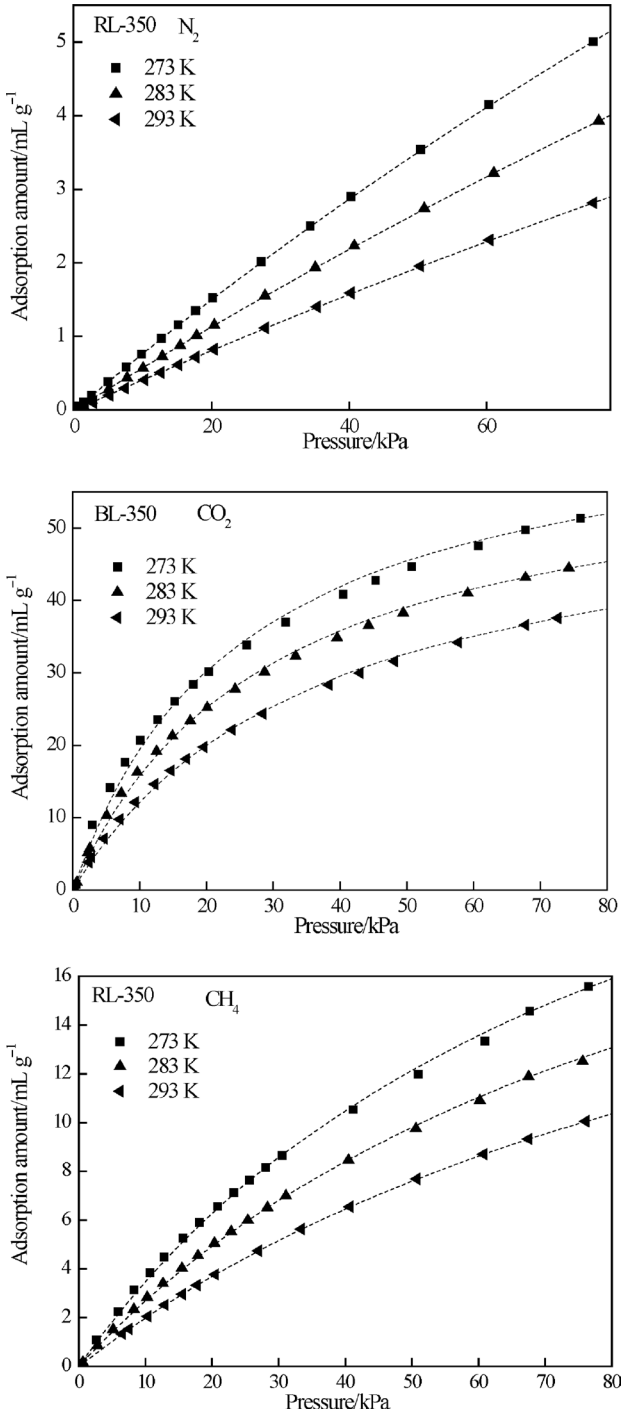

Fig. 6 – *Low-pressure isotherms for sorption of N_2, CH_4 and CO_2 onto RL-350 at low pressures; experimental data and Tóth model curves*

low 0.2 mmol g^{-1}. This suggests that more energetic sites for carbon dioxide, methane and nitrogen at low loading are filled preferentially with less active sites filled as adsorption proceeds. The modest decrease in isosteric enthalpy with increase in loading of RL-350 in adsorbing CO_2, CH_4 and N_2 indicates only mild heterogeneity for these three gases. The isosteric enthalpies of different gases on RL-350 are approximately 10 to 30 kJ mol^{-1}, which generally

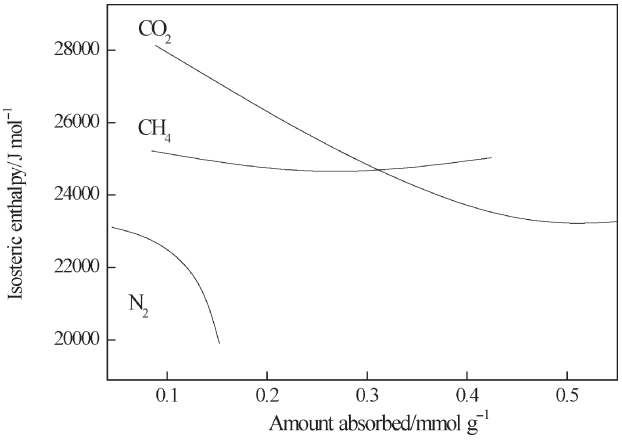

Fig. 7 – *Isosteric enthalpies of adsorption with respect to surface loading on RL-350*

falls below the range of isosteric enthalpies of physisorption of CO_2, CH_4 and N_2 on adsorbents such as activated carbon. This is consistent with the non-polar nature of the carbonaceous surface.

High-pressure adsorption of CO_2, CH_4, and N_2

In addition to the low-pressure adsorption, we also measured the high-pressure adsorption equilibrium of methane, carbon dioxide, and nitrogen on RL-350. We adopted the Peng-Robinson equation to determine fugacity and compressibility factor for those gases.

The high-pressure adsorption isotherms are shown in Fig. 8. The high-pressure isotherms obtained for carbon dioxide, methane and nitrogen onto RL-350 belong to type I of the IUPAC classification. At all pressures, carbon dioxide was the most strongly adsorbed gas, followed by methane and nitrogen.

Tóth equation was also chosen to model the high-pressure adsorption. The mathematical form of Tóth model at high pressure is as follows:

$$n^{\Omega} = \frac{n_m^* BP}{[1+(BP)^t]^{\frac{1}{t}}} = n + v_a \rho_g \tag{3a}$$

$$B = B^0 \exp\left(-\frac{\Delta H_0}{RT}\right) \tag{3b}$$

where n^{Ω} is the absolute amount adsorbed in mmol g^{-1}, n is the excess adsorption obtained from the measurement (mmol g^{-1}), n_m^* is the parameter that corresponds to full coverage of solid surface, v_a is the volume of adsorbate in the adsorbed phase in m^3 g^{-1}, ρ_g is the density of the bulk gas in mol m^{-3}, B and t are constants from Tóth equation. ΔH_0 is isosteric heat of adsorption at zero loading, B^0 is the infinite adsorption constant. We could obtain the

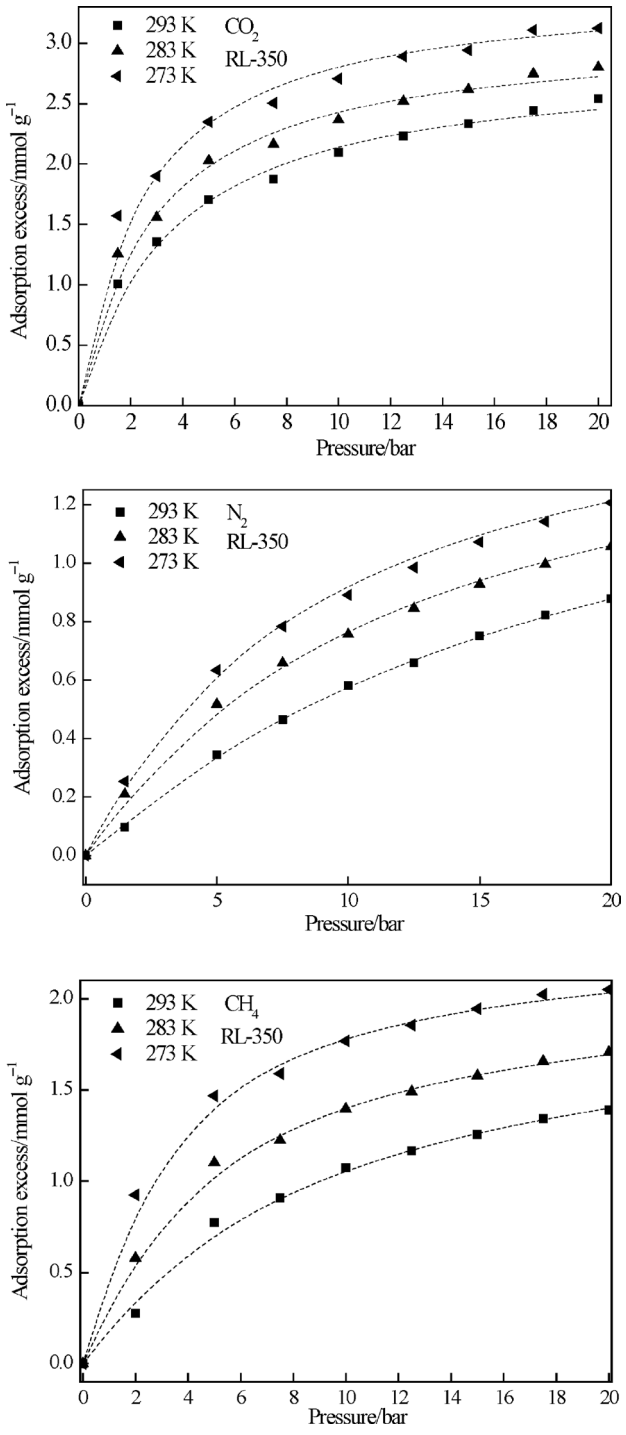

Fig. 8 – *Low-pressure isotherms for sorption of N_2, CH_4 and CO_2 onto RL-350 at high pressures; experimental data and Tóth model curves*

excessive adsorption formula to extrapolate the corresponding constants in equation:

$$n = \left(\frac{n_m^* Bf}{[1+(Bf)^t]^{\frac{1}{t}}} \right) \left(n_m^* - \frac{S^{3/2}}{\left(n_m^* A_v\right)^{1/2}} \rho_g \right) \qquad (4)$$

The detailed derivation of the model and definition of each constant could be found in literature.[15] By fitting the excess adsorption data of different gases onto RL-350 with eq. 4, we obtained the constants of Tóth equation, and Table 3 shows the isosteric heat of adsorption at zero loading, ΔH_0, and infinite adsorption constants B^0 of different gases. Fig. 8 shows that Tóth model is satisfactory in representing the experimental data of RL-350 in adsorbing carbon dioxide, methane and nitrogen under high pressure at different temperatures. The isosteric heat of adsorption with zero loading of RL-350 for adsorbing different gases is ordered as follows: carbon dioxide > methane > nitrogen, which generally agrees with the results calculated based on low-pressure equilibrium data.

Table 3 – *Constants of Tóth model for adsorption of CO_2, N_2 and CH_4 onto RL-350 at high pressure*

RL-350	Temperature	t	n_m^*	B^0	$-\Delta H_0$
Gas	K		mmol g^{-1}	atm	kJ mol^{-1}
CO_2	293	0.27	2.1	$4 \cdot 10^{-5}$	22
	283	0.27	2.3		
	273	0.25	2.6		
CH_4	293	0.58	1.3	$3 \cdot 10^{-5}$	17
	283	0.71	1.4		
	273	0.63	1.4		
N_2	293	0.42	1.7	$2 \cdot 10^{-3}$	11
	283	0.49	1.7		
	273	0.47	1.9		

The preferential adsorption of carbon dioxide indicates that RL-350 can be used for the separation of CO_2 from its mixture with methane and nitrogen. The variation of ideal selectivity of carbon dioxide relative to methane (n_{CO_2} / n_{CH_4}) and methane relative to nitrogen (n_{CH_4} / n_{N_2}) at 293 K are shown in Fig. 9. In Table 4, the ideal selectivities of n_{CO_2} / n_{CH_4} and n_{CH_4} / n_{N_2} on different commercial adsorbents are compared at room temperature at pressures below 5 bar. We see that the ideal selectivity n_{CO_2} / n_{CH_4} and n_{CH_4} / n_{N_2} of our samples is comparable to or even better than that of the commercial activated carbons, and carbon molecular sieves for preferentially adsorbing carbon dioxide to methane and nitrogen. Considering our less harsh preparation conditions (activation temperature below 400 °C) and relatively good CO_2 selectivity performance, our process shows a promising approach in preparing carbonaceous adsorbents for gas separation with low environmental impact.

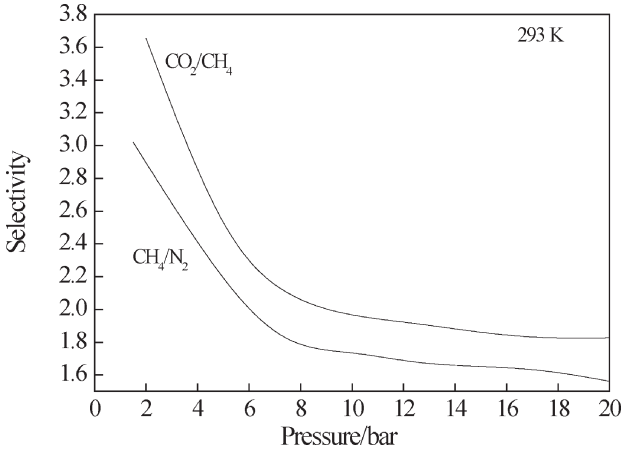

Fig. 9 – *RL-350 ideal selectivity (n_{CO_2} / n_{CH_4}) of carbon dioxide relative to methane and methane relative to nitrogen (n_{CH_4} / n_{N_2}) at 293 K*

Table 4 – *Comparison of the ideal selectivity of CO_2/CH_4 and CH_4/N_2 onto RL-350 at room temperature and 5 bar*

Sample	BET Specific Surface Area ($m^2\ g^{-1}$)	Ideal Selectivity CO_2/CH_4	Ideal Selectivity CH_4/N_2	Ref.
RL-350	405	3.0	1.5	This work
Zeolite 13X	–	3.3	1.5	16
Activated carbon	820	1.7	2.0	17
Commercial activated carbon	1250	–	2.2	18
Commercial activated carbon Norit R1	1450	1.6	–	19
Commercial activated carbon Maxsorb	3250	1.3	–	20
Carbon molecular sieve CMS	–	–	2.5	21
Activated carbon from biomass	645	–	2.0	22

Dynamic adsorption experiments of CO_2/CH_4 mixtures in the packed bed reactor

Although the equilibrium results indicate good ideal selectivity of prepared activated carbon towards CO_2/CH_4 mixtures, the dynamic adsorption experiments in the packed bed reactor were conducted to validate its potential for gas separation. In this paper, RL-350 was used in the packed bed reactor for dynamic separation of CO_2 from CH_4. The gas was considered to flow isothermally through the packed bed of spherical pellets; plug flow was supposed to be appropriate in our system. Mass balances for gases in the bed of porosity ε_b resulted in the following equation:

$$\varepsilon_b \frac{\partial c}{\partial t} + u\frac{\partial c}{\partial z} - D_z \frac{\partial^2 c}{\partial z^2} = -R \tag{5}$$

where c is concentration of adsorbent in the gas phase, D_z is the axial dispersion coefficient, u is the superficial fluid velocity. The terms on the left hand side are transient, flux and diffusion flux, respectively. The term on the right hand side is the source term, which represents the diffusion of the gas from bulk phase to the surface of the pores and is calculated as:

$$\varepsilon_p \frac{\partial c_p}{\partial t} + \rho_s \frac{\partial n_s}{\partial t} = \alpha k_{\text{overall}}(c - c_p) \tag{6}$$

where c and c_p are the concentration of adsorbent in the gas phase and the average concentration in the pores of the adsorbent, respectively, n_s is the average adsorbent loading, α is the specific surface area per unit bed volume, ρ_s is the adsorbent density, and k_{overall} is the overall mass transfer coefficient. The initial and boundary conditions appropriate for the breakthrough curve simulation are:

$$\begin{aligned} &c(t=0) = 0, \quad n_s(t=0) = 0, \quad c_p(t=0) = 0 \\ &c_0 + \frac{\partial c}{\partial z}\Big|_{z=0} = 0 \\ &\frac{\partial c}{\partial z}\Big|_{z=L} = 0 \end{aligned} \tag{7}$$

k_{overall} can be calculated as the sum of film and pore mass transfer coefficients. We used Sherwood number Sh to estimate the film coefficient as follows:

$$Sh = 2 + 1.1 Re^{0.6} Sc^{0.33} \tag{8}$$

where Re and Sc are Reynolds and Schmidt number, respectively. The pore mass transfer coefficient can be calculated as follows:

$$k_p = \frac{5\alpha}{r\tau\left(\frac{1}{D_k} + \frac{1}{D_m}\right)} \tag{9}$$

where r is the particle radius, D_k is Knudsen diffusivity, D_m is molecular diffusivity, τ is tortuosity factor, and Peclet number is used to calculate the dispersion coefficient D_z. Partial differential equations must be rearranged into the dimensionless form and the following dimensionless variables were used to make the governing equations dimensionless:

Gas concentration: $c^* = \frac{c}{c_0}$; $c_p{}^* = \frac{c_p}{c_0}$

Time: $t^* = \frac{t}{1/u_z}$

Distance in axial direction: $z^* = \frac{z}{l}$

Radius of pellet: $r^* = \frac{r}{r_p}$

The governing equations are then cast into the following form:

$$\frac{\partial c^*}{\partial t^*} + A\frac{\partial c^*}{\partial z^*} - \frac{1}{Pe}\frac{\partial^2 c^*}{\partial z^{*2}} + B(c^* - c^*_{\ p}) = 0 \quad (10)$$

$$\frac{\partial c_p^{\ *}}{\partial t^*} + C(c^* - c^*_{\ p}) = 0 \quad (11)$$

where A, B and C, respectively, are:

$$A = -\frac{1}{\varepsilon_b}, \quad (12)$$

$$B = \frac{15k_{overall}(1-\varepsilon_b)}{\varepsilon_b r_p u(k_{overall} + \frac{5\alpha}{\tau}(\frac{1}{D_k} + \frac{1}{D_m}))} \quad (13)$$

$$C = \frac{k_{\text{overall}} l}{\alpha u(k_{\text{overall}} + \frac{5\alpha}{\tau}(\frac{1}{D_k} + \frac{1}{D_m}))} \cdot \cdot [\frac{2N_m(1-\alpha)}{10^6 r^2_{\text{micro}}} - \frac{15(\frac{5\alpha}{\tau}(\frac{1}{D_k} + \frac{1}{D_m}))^2}{r_p^{\ 2}}] \quad (14)$$

N_m is the parameter that corresponds to full coverage of solid surface from Langmuir adsorption equation, r_{micro} is average micropore diameter, l is length of the bed.

Experimental breakthrough curves are shown in Fig. 10. The reasonable agreement is obtained between experimental results and our modeling indicating the acceptable approximation. Although our equilibrium results show ideal selectivity of CO_2/CH_4 in the range of approximately 3–3.6, the difference of the breakthrough time between CO_2 and CH_4 is not pronounced, indicating that the dynamic separation using the prepared RL-350 pellet performs relatively poorly in separating CO_2 and CH_4 using single adsorption bed reactor and experimental conditions investigated. This also indicates that the real selectivity of CO_2/CH_4 in the real dynamic separation is much less than 3–3.6. This may point to the need for further modification of the prepared carbon adsorbent e.g., by surface modification with functional groups or further modification of the process e.g., by increasing retention time in the column to increase the real selectivity of CO_2 vs. CH_4.

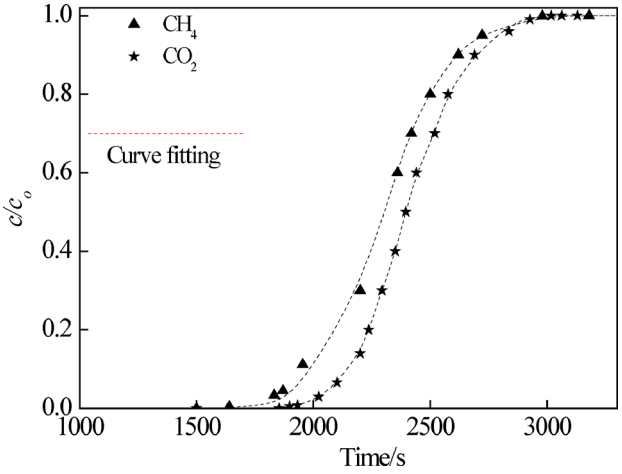

Fig. 10 – *Breakthrough curves for adsorption of CO_2 and CH_4 onto RL-350 at 298 K in the packed bed reactor; experimental data and model curves*

Conclusions

Carbon adsorbents were produced from biomass, i.e. from reed pulping black liquor by hydrothermal treatment at 200 °C followed by fast carbonization in fluidized bed at 350 °C for 5 minutes. The BET specific surface area of carbon at optimum conditions was 390 $m^2\ g^{-1}$. The adsorption of carbon dioxide, methane and nitrogen at pressures up to 2 MPa and at different temperatures was measured and represented with the Tóth equation together with Peng-Robinson equation of state for determination of the gas phase fugacity. The sample RL-350 showed good performance in preferential adsorption of CO_2 vs. CH_4 below 5 bar at 293 K. The calculated isosteric enthalpies of adsorption for different gases on RL-350 indicated mildly heterogeneous surfaces. The kinetic results indicate its potential for separation of carbon dioxide from carbon dioxide/methane mixture.

ACKNOWLEDGEMENTS

The National High Technology Research and Development Program 863 (2011AA060703) and Innovation funds of Institute of Processes Engineering of Chinese Academy of Sciences (No: 062702) are highly appreciated for their financial support.

References

1. *Sun, Y., Zhang, J. P., Yang, G., Li, Z. H.,* Spectrosc. Spect. Anal. **27** (2007) 1997.
2. *Sun, Y., Zhang, J. P., Yang, G., Li, Z. H.,* Spectrosc. Spect. Anal. **27** (2007) 371.
3. *Christopher J. B.,* Handbook of Pulping and Papermaking (Second Edition), 1996, pp 101-122.
4. *Naqvi, M. J., Yan, M. F.,* Bioresource. Technol. **101** (2010) 937.
doi: http://dx.doi.org/10.1016/j.biortech.2009.08.086

5. *Sricharoenchaikul, V.,* Bioresource. Technol. **100** (2009) 638.
doi: http://dx.doi.org/10.1016/j.biortech.2008.07.011
6. *Whitty, K., Backman, R., Hupa, M.,* Bioresource. Technol. **99** (2008) 663.
doi: http://dx.doi.org/10.1016/j.biortech.2006.11.065
7. *Lu, X. W., Jordan, B., Berge, N. D.,* Waste Manage. **32** (2012) 1353.
doi: http://dx.doi.org/10.1016/j.wasman.2012.02.012
8. *Kang, S. M., Li, X. L., Fan, J., Chang, J.,* Bioresource. Technol. **110** (2012) 715.
doi: http://dx.doi.org/10.1016/j.biortech.2012.01.093
9. *Sun, Y., Zhang, J. P., Yang, G., Li, Z. H.,* Chem. Biochem. Eng. Q. **21** (2007) 169.
10. *Sun, Y., Zhang, J. P., Yang, G., Li, Z. H.,* Environ. Technol. **28** (2007) 491.
doi: http://dx.doi.org/10.1080/09593332808618810
11. *Sun, Y., Zhang, J. P., Yang, G., Li, Z. H.,* Environ. Prog. **26** (2007) 78.
doi: http://dx.doi.org/10.1002/ep.10181
12. *Sun, Y., Yang, G. Wang, Y. S., Zhang, J. P.,* Environ. Prog. **30** (2011) 648.
doi: http://dx.doi.org/10.1002/ep.10503
13. *Ryu, J., Suh, Y. W., Suh D. J., Ahn, D. J.,* Carbon **48** (2010) 1990.
doi: http://dx.doi.org/10.1016/j.carbon.2010.02.006
14. *Sun, Y., Wei, J., Wang, Y. S., Yang, G., Zhang, J. P.,* Environ. Technol. **31** (2010) 53.
doi: http://dx.doi.org/10.1080/09593330903338411
15. *Zhou, L., Zhou, Y. P., Bai, S. P., Lu, C. Z., Yang, B.,* J. Colloid. Interface. Sci. **239** (2001) 33.
doi: http://dx.doi.org/10.1006/jcis.2001.7514
16. *Cavenati, S., Grande, C. A., Rodrigues, A. E.,* J. Chem. Eng. Data. **49** (2009) 1095.
doi: http://dx.doi.org/10.1021/je0498917
17. *Sun, Y., Yang, G., Zhang, J. P., Wang, Y. S., Yao, M. S.,* Chem. Eng. Technol. **35** (2012) 309.
doi: http://dx.doi.org/10.1002/ceat.201100309
18. *Ribeiro, R. P., Sauer, T. P., Lopes, F. V., Moreira, R. F., Grande, C. A., Rodrigues, A. E.,* J. Chem. Eng. Data. **53** (2008) 2311.
doi: http://dx.doi.org/10.1021/je800161m
19. *Choi, B. U., Choi, D. K., Lee, Y. W., Lee, B. K., Kim, S. H.,* J. Chem. Eng. Data. **48** (2003) 603.
doi: http://dx.doi.org/10.1021/je020161d
20. *Himeno, S., Komatsu, T., Fujita, S.,* J. Chem. Eng. Data. **50** (2005) 369.
doi: http://dx.doi.org/10.1021/je049786x
21. *Belmabkhout, Y., Weireld, G. D., Frere, M.,* J. Chem. Eng. Data. **49** (2003) 1379.
doi: http://dx.doi.org/10.1021/je049900b
22. *Shaheen, A. M.,* J. Chem. Eng. Data. **55** (2010) 313.
doi: http://dx.doi.org/10.1021/je900350k